Apo States of Calmodulin and CaBP1 Control Ca_V1 Voltage-Gated Calcium Channel Function through Direct Competition for the IQ Domain

Felix Findeisen [1,2], Christine H. Rumpf [1,2] and Daniel L. Minor Jr. [1,2,3,4]

*1 - **Cardiovascular Research Institute,** University of California, San Francisco, CA 94158-9001, USA*
*2 - **California Institute for Quantitative Biomedical Research,** University of California, San Francisco, CA 94158-9001, USA*
*3 - **Departments of Biochemistry and Biophysics,** and Cellular and Molecular Pharmacology, University of California, San Francisco, CA 94158-9001, USA*
*4 - **Physical Biosciences Science Division,** Lawrence Berkeley National Laboratory, Berkeley, CA 94720, USA*

Correspondence to Daniel L. Minor: *daniel.minor@ucsf.edu*
http://dx.doi.org/10.1016/j.jmb.2013.06.024
Edited by B. Poolman

Abstract

In neurons, binding of calmodulin (CaM) or calcium-binding protein 1 (CaBP1) to the Ca_V1 (L-type) voltage-gated calcium channel IQ domain endows the channel with diametrically opposed properties. CaM causes calcium-dependent inactivation and limits calcium entry, whereas CaBP1 blocks calcium-dependent inactivation (CDI) and allows sustained calcium influx. Here, we combine isothermal titration calorimetry with cell-based functional measurements and mathematical modeling to show that these calcium sensors behave in a competitive manner that is explained quantitatively by their apo-state binding affinities for the IQ domain. This competition can be completely blocked by covalent tethering of CaM to the channel. Further, we show that Ca^{2+}/CaM has a sub-picomolar affinity for the IQ domain that is achieved without drastic alteration of calcium-binding properties. The observation that the apo forms of CaM and CaBP1 compete with each other demonstrates a simple mechanism for direct modulation of Ca_V1 function and suggests a means by which excitable cells may dynamically tune Ca_V activity.

Introduction

High-voltage activated calcium channel (Ca_V) opening provides the primary source of calcium influx in excitable cells and couples electrical signals to chemical signaling cascades [1,2]. A set of calcium-dependent autoregulatory mechanisms shapes Ca_V activity in response to the influx of the permeant ion [3,4] and strongly affects neurotransmitter release, excitation–contraction coupling, and calcium-dependent gene activation [4,5]. Crucial among these activity-dependent changes is a process called calcium-dependent inactivation (CDI) that limits calcium entry following channel activation and for which the calcium sensor protein calmodulin (CaM) is essential [3,4,6,7].

Ca_Vs are multi-subunit complexes of four main components [8,9]: a pore-forming Ca_V1 (L-type) or Ca_V2 (P/Q-, N-, and R-type) $Ca_V\alpha_1$ subunit [1], a cytoplasmic $Ca_V\beta$ subunit [10,11], the membrane anchored subunit $Ca_V\alpha_2\delta$ [12], and CaM [13]. In some neurons, members of a family of neuronal calcium sensor proteins similar to CaM, known as CaBPs [14], can replace CaM [15]. This calcium sensor exchange creates Ca_Vs having strikingly different functional properties from those under the control of CaM [16–22]. In particular, $Ca_V1.2$ [19,22,23] and $Ca_V1.3$ [16,17] lack CDI when calcium-binding protein 1 (CaBP1), a CaBP highly expressed in the brain and retina [15], is part of the channel complex. CaM and CaBP1 are calcium-binding proteins comprising two lobes each bearing a pair of EF hands and an interlobe flexible linker [15,23,24]. Structural studies have shown that the calcium-bound forms of the CaM and CaBP1 C-terminal lobes (C-lobes) have similar three-dimensional structures [23,24] and compete for binding to the same channel element, the IQ domain [23], whereas the N-terminal lobes (N-lobes) are more divergent [23].

Although multiple Ca_V1 channel segments have been implicated in CaM and CaBP1 function

[25–29], the main attachment point for both is the IQ domain of the $Ca_V\alpha_1$ C-terminal cytoplasmic tail [6,17,19,25]. Previous studies have shown that CaBP1 and CaM cannot simultaneously bind the $Ca_V1.2$ IQ domain [17,19,23]; however, evidence for functional competition in the full-length channel has been lacking. Here, we use thermodynamic measurements to investigate the CaM and CaBP1 competition on the $Ca_V1.2$ IQ domain. Our data show that this competition occurs between apo states of the respective molecules and that although their IQ domain binding sites overlap, the two calcium sensor proteins bind in different ways. Further, we present experiments using *Xenopus* oocytes that corroborate these biochemical observations and that demonstrate that CaM and CaBP1 can compete directly for control of $Ca_V1.2$ CDI in living cells. Importantly, mathematical modeling of the CaM-CaBP1 competition based on the isothermal titration calorimetry (ITC) measurements predicts the functional competition measured on full-length channels in the context of a cell membrane. This excellent agreement, which emerges from analysis of measurements made in dramatically different milieus, indicates that the simplified biochemical systems investigated here capture the essence of the mechanism by which CaM and CaBP1 competitively alter channel function.

Results

Ca^{2+}/CaM has sub-picomolar affinity for the $Ca_V1.2$ IQ domain

The $Ca_V1.2$ IQ domain is the main binding site for both Ca^{2+}/CaM [6,7] and Ca^{2+}/CaBP1 [19]. Previous ITC studies have determined the binding affinities of the individual CaBP1 lobes, N-$lobe_{CaBP1}$, and Ca^{2+}/C-$lobe_{CaBP1}$ [23]; full-length Ca^{2+}/CaBP1 [23]; and the individual Ca^{2+}/CaM lobes, Ca^{2+}/N-$lobe_{CaM}$, and Ca^{2+}/C-$lobe_{CaM}$ [30] for this portion of the $Ca_V1.2$ C-terminal tail; however, measurement of the affinity of full-length Ca^{2+}/CaM for the $Ca_V1.2$ IQ domain had remained elusive. Hence, we set out to examine this interaction using ITC.

Direct titration of Ca^{2+}/CaM into solution containing the $Ca_V1.2$ IQ domain yielded a complex curve (Fig. 1a) that could not be explained by a single binding event. ITC analysis of Ca^{2+}/CaBP1 with the $Ca_V1.2$ IQ domain binding posed similar difficulties that were surmounted using a displacement titration strategy coupled with thermodynamic cycle analysis [23]. Therefore, we tested if a comparable approach would apply here. Indeed, titration of Ca^{2+}/CaM into a preformed Ca^{2+}/C-$lobe_{CaM}$:$Ca_V1.2$ IQ domain complex gave a single transition (Fig. 1b). As the affinity of the Ca^{2+}/C-$lobe_{CaM}$:$Ca_V1.2$ IQ binding reaction is known [30], we could use a thermodynamic cycle (Fig. 1c) together with competition ligand binding by displacement analysis [31] to determine the affinity of full-length Ca^{2+}/CaM for the $Ca_V1.2$ IQ domain. Importantly, there is no detectable interaction between Ca^{2+}/CaM and Ca^{2+}/C-$lobe_{CaM}$ that could interfere with the analysis (Fig. 1d).

We find that the affinity of Ca^{2+}/CaM for the $Ca_V1.2$ IQ domain is exceptionally high, K_d = 850 ± 130 fM, a result that agrees with a previously reported sub-picomolar estimate of this interaction [32]. The affinity of Ca^{2+}/CaM for the $Ca_V1.2$ IQ domain is ~3100-fold stronger than that of Ca^{2+}/C-$lobe_{CaM}$ (Table 1) and indicates that there is a substantial contribution from the Ca^{2+}/N-$lobe_{CaM}$ that agrees with its extensive $Ca_V1.2$ IQ domain contacts [30,33]. Although extreme, the sub-picomolar affinity of Ca^{2+}/CaM for the $Ca_V1.2$ IQ domain is within the bounds other tight Ca^{2+}/CaM:peptide interactions (cf. a CaM kinase II peptide, 70 fM) [34] but is many orders of magnitude greater than what Ca^{2+}/CaM displays for the IQ domain of the distantly related voltage-gated sodium channel $Na_V1.5$ (2 μM) [35] and the $Na_V1.5$ III–IV loop (3 μM) [36].

Our previous ITC studies using buffer conditions identical with those used here showed that Ca^{2+}/CaBP1 binds strongly to the $Ca_V1.2$ IQ domain (290 ± 0 pM) [23]. Nevertheless, this value is ~340-fold weaker than the Ca^{2+}/CaM:$Ca_V1.2$ IQ domain interaction. In good agreement with these findings, Ca^{2+}/CaBP1 was unable to displace Ca^{2+}/CaM from a preformed Ca^{2+}/CaM:$Ca_V1.2$ IQ domain complex (Fig. 1e). This result disagrees with the results reported in pull-down studies of Zhou *et al.* [19]; however, the discrepancy is readily explained by the fact that Zhou *et al.* [19] used a $Ca_V1.2$ IQ domain construct lacking several key residues that interact with Ca^{2+}/CaM, including two that bind Ca^{2+}/N-$lobe_{CaM}$ (cf. Ref. [30]).

Taken together, these ITC experiments establish that Ca^{2+}/CaM binds the $Ca_V1.2$ IQ domain with an exceptionally high affinity that is several hundred-fold stronger than that of Ca^{2+}/CaBP1 (Table 1). As the affinity of the individual Ca^{2+}/C-lobes differs only threefold [23,30], the competitive advantage of Ca^{2+}/CaM over Ca^{2+}/CaBP1 for the $Ca_V1.2$ IQ domain is almost exclusively due to differences in the contributions from the Ca^{2+}/N-lobe.

apo-CaBP1 binds the $Ca_V1.2$ IQ domain more strongly than apo-CaM

The large affinity differences of Ca^{2+}/CaM and Ca^{2+}/CaBP1 for the $Ca_V1.2$ IQ domain preclude effective competition by Ca^{2+}/CaBP1. However, because Ca^{2+}/CaM and Ca^{2+}/CaBP1 are likely to be present only for brief periods when local calcium levels rise due to channel activity, we reasoned that

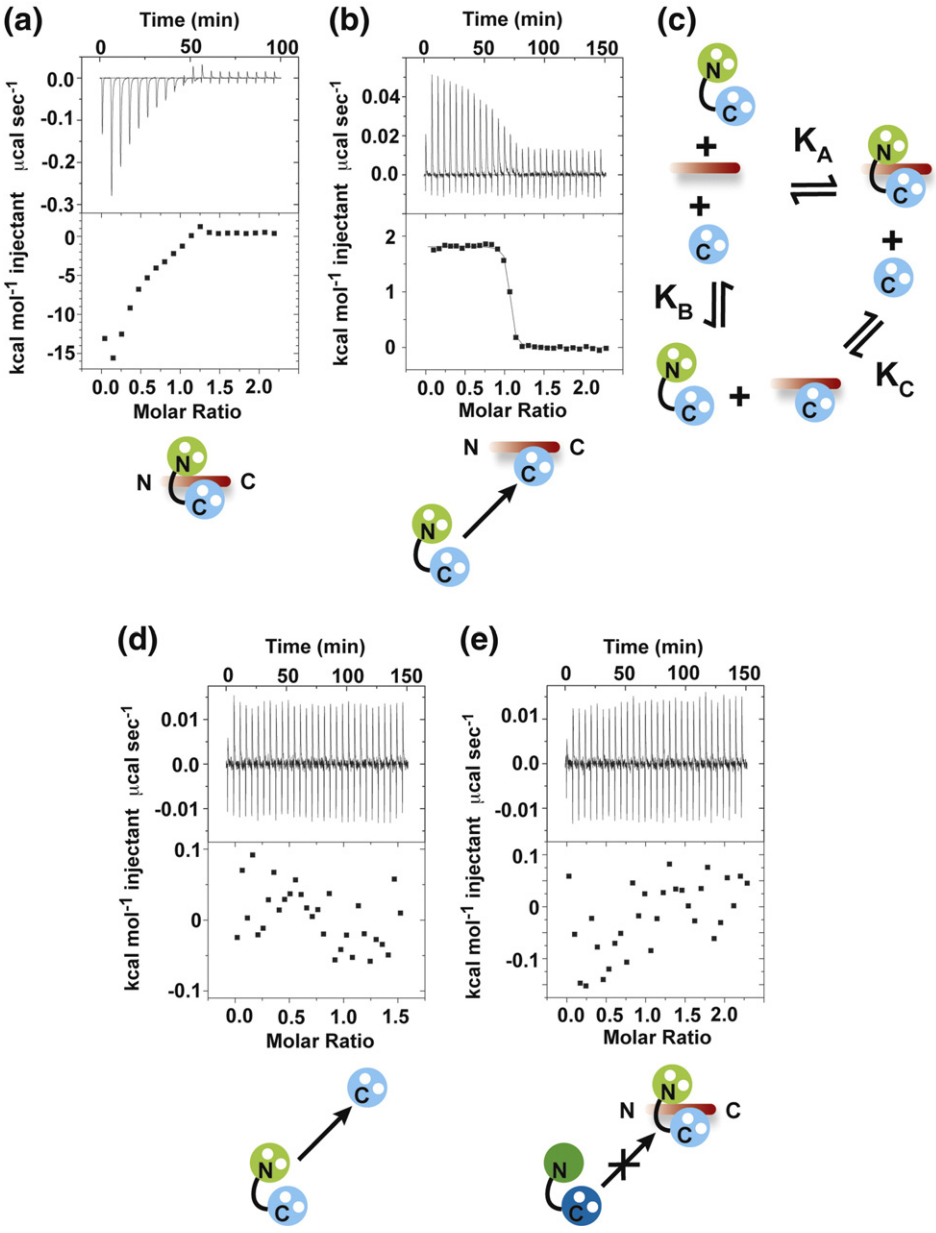

Fig. 1. Characterization of $Ca^{2+}{}_4$:CaM-$Ca_V1.2$ IQ domain binding. Exemplar ITC titrations for (a) 75 µM $Ca^{2+}{}_4$:CaM into 7.5 µM $Ca_V1.2$ IQ domain and (b) 75 µM $Ca^{2+}{}_4$:CaM into 7.5 µM $Ca_V1.2$ IQ domain and 50 µM $Ca^{2+}{}_2$:C-$lobe_{CaM}$. (c) Thermodyamic cycle for analysis of the binding of $Ca^{2+}{}_4$:CaM (K_A) to the $Ca_V1.2$ IQ domain. K_B describes $Ca^{2+}{}_2$:C-$lobe_{CaM}$ binding. K_C describes the competition of $Ca^{2+}{}_2$:C-$lobe_{CaM}$ by CaM. Exemplar ITC titrations for (d) 75 µM $Ca^{2+}{}_4$:CaM into 50 µM $Ca^{2+}{}_2$:C-$lobe_{CaM}$ and (e) 75 µM $Ca^{2+}{}_2$:CaBP1 into 7.5 µM $Ca_V1.2$ IQ domain and 11.25 µM $Ca^{2+}{}_4$:CaM. Icons depict ITC components. N-lobes and C-lobes are green and blue, respectively. CaM and CaBP1 are in pastel and dark shades, respectively. White spheres represent Ca^{2+}. $Ca_V1.2$ IQ domain is shown in red.

the physiologically relevant competition for the $Ca_V1.2$ IQ domain might occur in the calcium-free, apo states of the respective calcium sensors. To look for biochemical evidence that could test this idea, we measured the affinities for the $Ca_V1.2$ IQ domain of a set of apo-CaM and apo-CaBP1 mimics. In each, we disabled calcium binding through an established strategy in which alanine replaces the first aspartate of the EF-hand consensus sequence [6,7,30]. "EF##" denotes which EF hands carry this change.

Because of limitations on reaching sufficient apo-lobe mimic concentrations for direct titration due to the weak nature of the interaction (K_d values $\geq$ 100 nM), which would have required concentrations of titrant and target that are not physically well behaved

Table 1. Titration calorimetry data for interactions between CaM and CaBP1 with the $Ca_V1.2$ IQ domain

	n	Setup	*N*	K_d (M)	ΔH (kcal mol^{-1})	ΔS (cal mol^{-1} K^{-1})	ΔG (kcal mol^{-1})	$K_{d,CaBP1}/K_{d,CaM}$	K_d(apo)/K_d (Ca^{2+})	$\Delta\Delta G$ (kcal mol^{-1})
N-lobe$_{BP}$ [a]	3	S	0.82 ± 0.05	$1.10 \times 10^{-6} \pm 8.0 \times 10^{-8}$	2.09 ± 0.40	34.5 ± 1.5	−7.84 ± 0.04	—	—	—
Ca^{2+}/C-lobe$_{BP}$ [a]	4	S	0.90 ± 0.07	$1.05 \times 10^{-8} \pm 1.9 \times 10^{-9}$	−2.88 ± 0.19	25.5 ± 0.6	−10.52 ± 0.11	—	—	—
Ca^{2+}/CaBP1 [a]	2	D	[b]	$2.9 \times 10^{-10} \pm 7.0 \times 10^{-11}$	−4.72 ± 0.07	26.6 ± 0.7	−12.38 ± 0.14	—	—	—
Ca^{2+}/N-lobe$_{CaM}$ [c]	2	S	0.85 ± 0.05	$5.76 \times 10^{-8} \pm 3.55 \times 10^{-8}$	−1.91 ± 0.14	26.7 ± 0.9	−9.60 ± 0.38	19	—	—
Ca^{2+}/C-lobe$_{CaM}$ [c]	2	S	0.98 ± 0.18	$2.63 \times 10^{-9} \pm 7.0 \times 10^{-11}$	−6.77 ± 0.21	14.2 ± 0.9	−11.31 ± 0.01	4.0	—	—
Ca^{2+}/CaM	2	D	[b]	$8.5 \times 10^{-13} \pm 1.3 \times 10^{-13}$	−5.74 ± 0.35	34.5 ± 0.9	−15.68 ± 0.08	340	—	—
N-lobe$_{BP}$ [a]	3	S	0.82 ± 0.05	$1.10 \times 10^{-6} \pm 8.0 \times 10^{-8}$	2.09 ± 0.40	34.5 ± 1.5	−7.84 ± 0.04	—	1	0
C-lobe $_{CaBP1}$EF34	2	D	[b]	$3.80 \times 10^{-6} \pm 1.30 \times 10^{-6}$	3.77 ± 0.20	37.7 ± 1.4	−7.08 ± 0.21	—	360	−3.44
CaBP1EF34	2	D	[b]	$9.1 \times 10^{-8} \pm 1.3 \times 10^{-8}$	−0.82 ± 0.15	29.0 ± 0.2	−9.15 ± 0.08	—	310	−3.24
N-lobe $_{CaM}$EF12	2	D	[b]	$>5 \times 10^{-6}$	n/a	n/a	> −6.9	<0.2	>90	< −2.78
C-lobe$_{CaM}$EF34	2	D	[b]	$2.2 \times 10^{-6} \pm 1.0 \times 10^{-8}$	−3.79 ± 0.06	12.4 ± 0.2	−7.34 ± 0.02	1.7	840	−4.05
CaMEF1234	2	D	[b]	$5.8 \times 10^{-7} \pm 5.0 \times 10^{-8}$	−3.36 ± 0.02	16.5 ± 0.2	−8.10 ± 0.06	0.14	680,000	−7.58

$\Delta\Delta G = RT\ln(K_d(apo)/K_d)$ (Ca^{2+}), where T = 288 K.
S, simple titration; D, displacement titration.
n denotes the number of independent experiments.
n/a, not applicable.
[a] Data from Ref. [23].
[b] *N* was set to 1.
[c] Data from Ref. [30].

(~500 μM), we derived the apo-CaM lobe (N-lobe$_{CaM}$EF12 and C-lobe$_{CaM}$EF34) and apo-CaBP1 C-lobe (C-lobe$_{CaBP1}$EF34) affinities for the $Ca_V1.2$ IQ domain using displacement ITC (Fig. 2a–c) and an analysis similar to Fig. 1c. These experiments showed that loss of calcium binding capacity in the individual CaM lobes caused a 2–3 order of magnitude affinity reduction relative to the calcium-bound forms: 2200 ± 10 nM *versus* 2.63 ± 0.07 nM for C-lobe$_{CaM}$EF34 and Ca^{2+}/C-lobe$_{CaM}$ and >5000 nM *versus* 57.6 ± 35.5 nM for N-lobe$_{CaM}$EF12 and Ca^{2+}:N-lobe$_{CaM}$, respectively (Fig. 2a and b; Table 1). We measured a similar magnitude change for the only CaBP1 lobe that responds to calcium [37], C-lobe$_{CaBP1}$, (3800 ± 1300 nM *versus* 10.5 ± 1.9 nM, for C-lobe$_{CaBP1}$EF34 and Ca^{2+}/C-lobe$_{CaBP1}$, respectively) (Fig. 2c; Table 1). Thus, the importance of calcium for elevating $Ca_V1.2$ IQ domain binding affinity is shared among the calcium responsive lobes of both CaM and CaBP1.

We also performed competition ITC experiments using apo-mimics of full-length CaM and CaBP1 (CaMEF1234 and CaBP1EF34) (Fig. 2d and e; Table 1). These revealed that in the case of CaM, the large change in affinity for the $Ca_V1.2$ IQ domain relative to the calcium-bound forms is greatly accentuated in the context of the full-length protein, reaching an ~6 orders of magnitude difference (580 ± 50 nM *versus* 850 ± 130 fM for CaMEF1234 and Ca^{2+}/CaM, respectively) (Fig. 2d and Table 1). In contrast, the ~300-fold difference for CaBP1 (91 ± 13 nM *versus* 290 ± 70 pM for CaBP1EF34 and Ca^{2+}/CaBP1; Fig. 2e and Table 1) is similar to that of C-lobe$_{CaBP1}$ alone and is consistent with the inability of N-lobe$_{CaBP1}$ to undergo a calcium-dependent conformational change [23]. The apo-CaM mimic affinity for the $Ca_V1.2$ IQ domain is close to that reported using in-cell fluorescence (1035 nM) [38] but in poorer agreement with estimates from *in vitro* fluorescence (~50 nM) [39]. Strikingly, comparison of the apo-state affinities shows that unlike in the calcium-bound states where Ca^{2+}/CaM has a huge advantage over Ca^{2+}/CaBP1, the $Ca_V1.2$ IQ domain favors binding of apo-CaBP1 by ~7-fold over apo-CaM. Thus, the data suggest that under calcium concentrations that favor the apo states, CaBP1 could compete effectively with CaM for binding to the $Ca_V1.2$ IQ domain.

Consequences of CaM-IQ domain affinity for calcium binding

Numerous studies have shown that target engagement can have strong effects on the apparent affinity of CaM for calcium due to thermodynamic linkage [32,40,41]. In this context, the nearly million-fold affinity difference between apo-CaM and Ca^{2+}/CaM for the $Ca_V1.2$ IQ domain was surprising. As

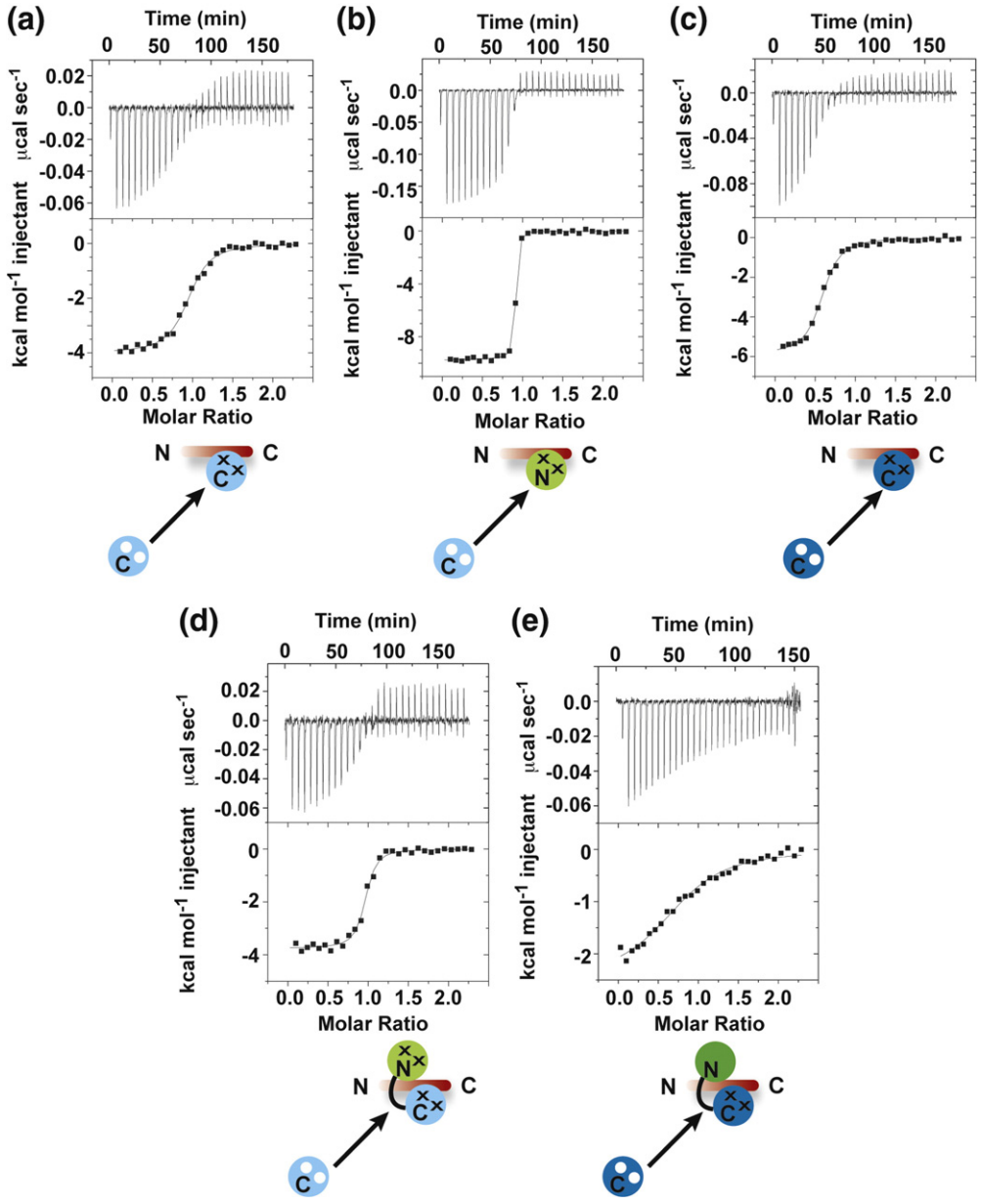

Fig. 2. Characterization of apo-CaM and apo-CaBP1 $Ca_V1.2$ IQ domain binding. Exemplar ITC titrations for the following: (a) 75 µM $Ca^{2+}{}_2$:C-$lobe_{CaM}$ into 7.5 µM $Ca_V1.2$ IQ domain and 50 µM C-$lobe_{CaM}$ EF34. (b) 75 µM $Ca^{2+}{}_2$:C-$lobe_{CaM}$ into 7.5 µM $Ca_V1.2$ IQ domain and 50 µM N-$lobe_{CaM}$EF12. (c) 75 µM $Ca^{2+}{}_2$:C-$lobe_{CaBP1}$ into 7.5 µM $Ca_V1.2$ IQ domain and 50 µM C-$lobe_{CaBP1}$EF34. (d) 75 µM $Ca^{2+}{}_2$:C-$lobe_{CaM}$ into 7.5 µM $Ca_V1.2$ IQ domain and 50 µM CaMEF1234. (e) 75 µM $Ca^{2+}{}_2$:C-$lobe_{CaBP1}$ into 7.5 µM IQ domain and 50 µM CaBP1EF34. Icons depict ITC components. N-lobes and C-lobes are green and blue, respectively. CaM and CaBP1 are in pastel and dark shades, respectively. White spheres represent Ca^{2+}. Black crosses indicate mutated EF hands. $Ca_V1.2$ IQ domain is shown in red.

the average affinity of CaM for calcium has been measured to be ~15 µM [42,43], the large differences associated with IQ domain engagement could be taken to suggest that the calcium affinity of IQ domain bound CaM might be shifted into the picomolar range. Such a scenario would cause IQ domain-bound CaM to remain in the calcium-bound form even at resting levels of intracellular calcium, which are ~100 nM [2,44]. This would put CaM far outside of the range where it could act as a physiologically relevant sensor for calcium-dependent control of channel function.

To try to understand this situation from a quantitative perspective, we constructed a model to evaluate how the measured large changes in protein–protein interactions might lead to changes

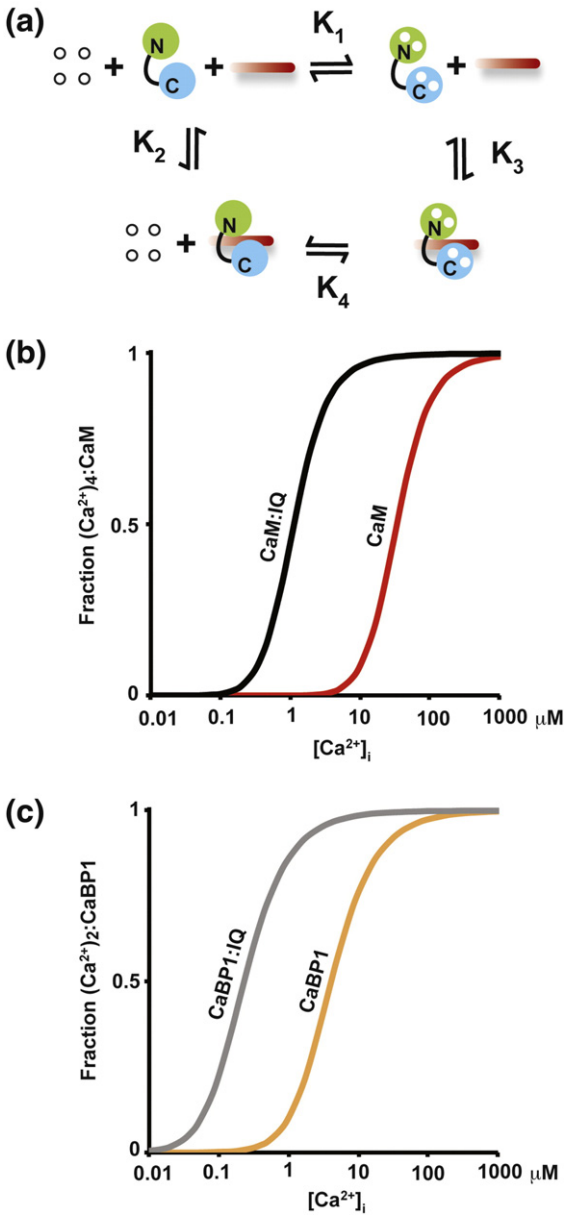

Fig. 3. Thermodynamic analysis of CaM, Ca^{2+}, and IQ domain binding. (a) Macroscopic thermodynamic cycle for CaM, Ca^{2+} and $Ca_V1.2$ IQ domain. K_1 and K_4 describe Ca^{2+} binding to CaM and the CaM/IQ complex, respectively. K_2 and K_3 describe IQ domain binding to calcium-free CaM and $Ca^{2+}{}_4$:CaM, respectively. (b) Calculated fraction of $Ca^{2+}{}_4$:CaM as a function of Ca^{2+} concentration for CaM alone (red) or bound to the IQ domain (black curve). (c) Calculated fraction of $Ca^{2+}{}_2$:CaBP1as a function of Ca^{2+} concentration for CaBP1 alone (orange) or bound to the IQ domain (gray curve).

in the free energy of calcium binding (Fig. 3a and Appendix A). This analysis shows that there needs to be only an ~30-fold increase (~1.9 kcal mol^{-1}) in the calcium affinity of each CaM EF hand to account for the approximately million-fold (~7.7 kcal mol^{-1}) affinity difference measured for the binding of apo-CaM and Ca^{2+}/CaM to the $Ca_V1.2$ IQ domain. Notably, this relative 30-fold change in Ca^{2+} affinity does not depend on the exact Ca^{2+} affinities of free CaM. This calcium affinity change is in good agreement with experimental estimates based on CaM:$Ca_V1.2$ IQ association [39]. The rather modest calcium affinity change arises from the fact that the reaction order is higher than a simple single binding event. The affinities of the four EF hands of CaM have been determined in a number of studies (e.g., Refs. [42,45,46]). Taking the values that have been used extensively for modeling studies [42] (e.g., Refs. [47,48]) and the affinity change caused by association with the $Ca_V1.2$ IQ domain, we calculated the fraction of $Ca^{2+}{}_4$:CaM present in both the free and $Ca_V1.2$ IQ domain-associated forms (Fig. 3b). Interestingly, the model indicates that the association of CaM with IQ domain shifts the sensitivity of the CaM calcium response from a range of 10–500 μM to 0.3–10 μM. Such a tuning of calcium sensitivity positions the complex perfectly in the range of physiologically relevant intracellular calcium changes [2,43,44].

Consequences of CaBP1-IQ domain affinity for calcium binding

Functional EF hands are not required for CaBP1 to inhibit CDI [23]. Nevertheless, given the differences of binding affinity for the $Ca_V1.2$ IQ domain between apo-CaBP1 and Ca^{2+}/CaBP1, which are considerably smaller than those for CaM but are still substantial (Table 1), we performed an equivalent mathematical analysis to consequences of IQ domain binding for the EF-hand affinities for CaBP1 (Appendix B). This analysis shows that association with the $Ca_V1.2$ IQ domain alters the affinity of each CaBP1 EF-hand for Ca^{2+} by 18-fold. This relative change in Ca^{2+} affinity upon IQ domain is independent of the absolute Ca^{2+} affinity of free CaBP1. Thus, despite the dramatically smaller change in IQ domain affinity between apo- and Ca^{2+}-bound forms of CaBP1 relative to CaM (310 *versus* 680,000), the fact that there are fewer EF hands in CaBP1 compared to CaM (2 rather than 4) results in affinity changes for each individual EF hand that are similar for CaBP1 and CaM (18 and 29, respectively). Taking the reported dissociation constants of the individual CaBP1 Ca^{2+} binding sites [37], similar to the analysis with CaM, we determined the fraction of the $Ca^{2+}{}_2$:CaBP1 form of CaBP1 as a function of calcium concentration in both the free and $Ca_V1.2$ IQ domain-bound forms (Fig. 3d). The reported apparent affinity of free CaBP1 compared to Ca^{2+} is ~10-fold stronger than that of free CaM. Provided that the affinity changes caused by IQ domain binding are distributed equally among the EF

hands, the analysis indicates that this rank order is maintained upon IQ domain binding and that the CaBP1:$Ca_V1.2$ IQ domain complex will bind Ca^{2+} at lower calcium concentrations than the CaM:$Ca_V1.2$ IQ domain complex.

CaBP1 and CaM binding sites comprise different $Ca_V1.2$ IQ domain elements

Previous studies have shown that the Ca^{2+}/C-lobes of CaM and CaBP1 have similar structures [23,24] and compete for overlapping binding sites on the $Ca_V1.2$ IQ domain [23]. Given the substantial difference in affinities between the calcium-bound forms of full-length CaM and CaBP1 for the $Ca_V1.2$ IQ domain (Table 1), we were interested in defining the structural basis for these differences. Ca^{2+}/CaM engages the $Ca_V1.2$ IQ domain using a set of six aromatic anchor residues that are divided into two categories based upon the Ca^{2+}/CaM lobe they contact [30]: $Ca_V1.2$ F1618, F1619, and Y1622 anchor Ca^{2+}/N-$lobe_{CaM}$; $Ca_V1.2$ Y1627, F1628, and F1631 anchor Ca^{2+}/C-$lobe_{CaM}$. Hence, removal of the Ca^{2+}/N-lobe anchors should

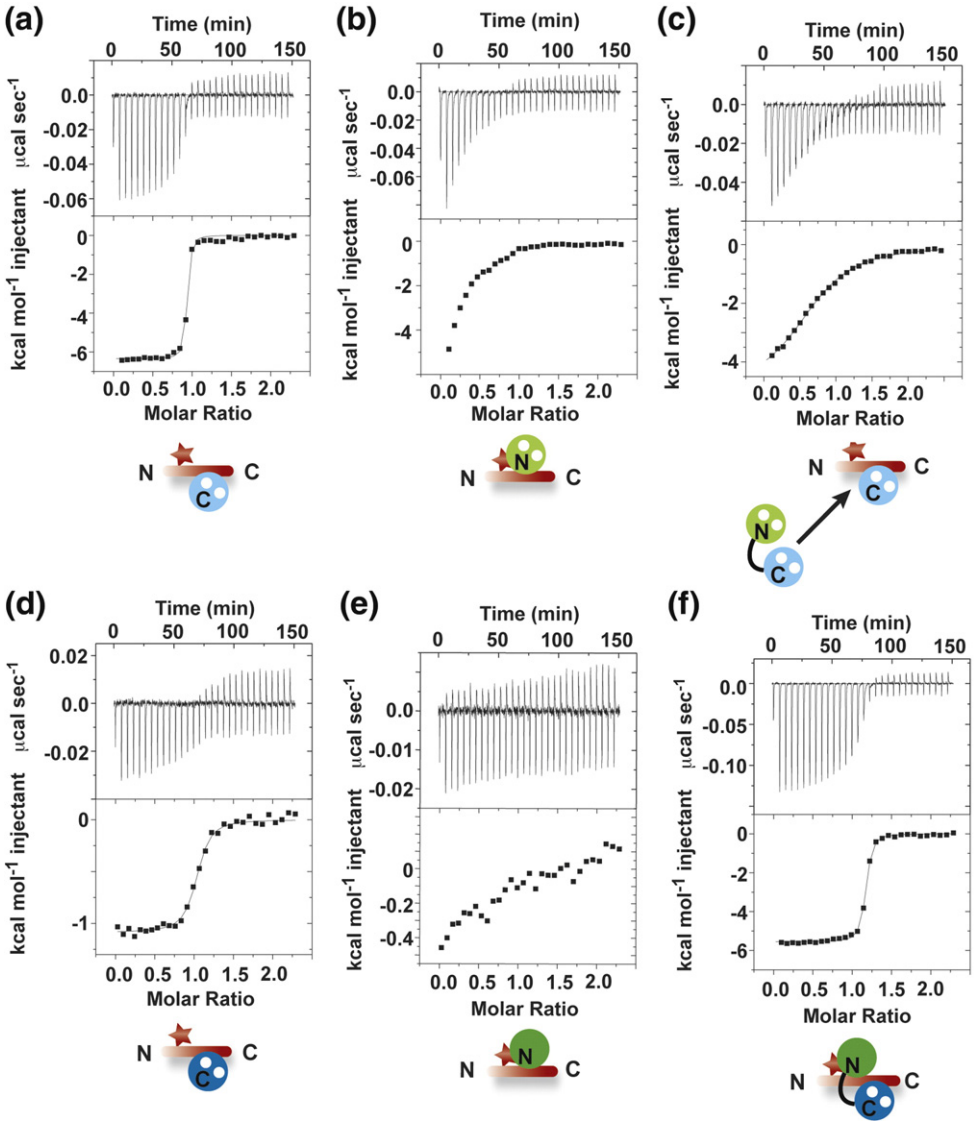

Fig. 4. Characterization of CaM and CaBP1 binding to the $Ca_V1.2$ IQ domain mutant "TripleA". Exemplar ITC titrations for the following: (a) 75 µM $Ca^{2+}{}_2$:C-$lobe_{CaM}$ into 7.5 µM TripleA. (b) 75 µM $Ca^{2+}{}_2$:N-$lobe_{CaM}$ into 7.5 µM TripleA. (c) 75 µM $Ca^{2+}{}_4$:CaM into 7.5 µM TripleA and 50 µM $Ca^{2+}{}_2$:C-$lobe_{CaM}$. (d) 75 µM $Ca^{2+}{}_2$:C-$lobe_{CaBP1}$ into 7.5 µM TripleA. (e) 75 µM $Ca^{2+}{}_2$:CaBP1 into 7.5 µM TripleA. (f) 75 µM $Ca^{2+}{}_2$:N-$lobe_{CaM}$ into 7.5 µM TripleA. Icons depict ITC components. N-lobes and C-lobes are in green and blue, respectively. CaM and CaBP1 are in pastel and dark shades, respectively. White spheres represent Ca^{2+}. $Ca_V1.2$ IQ domain is shown in red. Red star signifies the TripleA mutation.

Table 2. Titration calorimetry data for interactions between CaM and CaBP1 with $Ca_V1.2$ IQ domain TripleA

	n	Setup	*N*	K_d (M)	ΔH (kcal mol^{-1})	ΔS (cal mol^{-1} K^{-1})	ΔG (kcal mol^{-1})	$K_{d,IQAAA}/K_{d,IQ}$	$\Delta\Delta G$ (kcal mol^{-1})
N-lobe$_{CaBP1}$	2	S	n/a	$>5 \times 10^{-6}$	n/a	n/a	>-6.9	>4.5	<-0.9
Ca^{2+}/C-lobe$_{CaBP1}$	2	S	0.93 ± 0.01	$2.21 \times 10^{-7} \pm 1.4 \times 10^{-8}$	−1.45 ± 0.14	25.5 ± 0.6	−8.65 ± 0.03	21	−1.87
Ca^{2+}/CaBP1	2	S	0.89 ± 0.19	$1.09 \times 10^{-8} \pm 2.0 \times 10^{-9}$	−4.77 ± 1.04	19.4 ± 4.0	−10.35 ± 0.11	38	−2.03
Ca^{2+}/N-lobe$_{CaM}$	2	S	n/a	$>5 \times 10^{-6}$	n/a	n/a	>-6.9	>90	<-2.7
Ca^{2+}/C-lobe$_{CaM}$	2	S	0.90 ± 0.01	$1.54 \times 10^{-9} \pm 2.1 \times 10^{-10}$	−6.44 ± 0.13	18.0 ± 0.1	−11.45 ± 0.08	0.6	0.14
Ca^{2+}/CaM	2	D	n/a[a]	$1.7 \times 10^{-10} \pm 2.0 \times 10^{-11}$	−10.6 ± 0.4	7.4 ± 1.6	−12.68 ± 0.07	200	−3.00

$\Delta\Delta G = RT\ln(K_{d,IQAAA}/K_{d,IQ})$, where $T = 288$ K.
S, simple titration; D, displacement titration.
n indicates the number of independent experiments.
n/a, not applicable.
[a] *N* was set to 1.

reduce the affinity of Ca^{2+}/CaM for the IQ domain while leaving the affinity for the Ca^{2+}/C-lobe$_{CaM}$ unaffected.

To test this idea, we used ITC to determine the affinity of full-length Ca^{2+}/CaM and its individual lobes for a mutant of the $Ca_V1.2$ IQ domain having the three Ca^{2+}/N-lobe$_{CaM}$ anchors replaced by alanine ($Ca_V1.2$ IQ TripleA). In agreement with the predictions from the structure, ITC shows that Ca^{2+}/C-lobe$_{CaM}$ binds to $Ca_V1.2$ IQ TripleA (Fig. 4a) and has an affinity (1.5 ± 0.2 nM, $\Delta\Delta G = 0.14$ kcal mol^{-1}) and thermodynamic parameters unchanged from wild type [30] (Tables 1 and 2). In contrast, ITC using Ca^{2+}/N-lobe$_{CaM}$ (Fig. 4b) revealed an affinity for $Ca_V1.2$ IQ TripleA that was greatly compromised by the loss of the N-lobe anchors (>5 μM, $\Delta\Delta G < -2.7$ kcal mol^{-1}) (Tables 1 and 2). In accord with these results, ITC measurements show that the TripleA mutation also reduced the affinity of full-length Ca^{2+}/CaM (170 ± 20 pM, $\Delta\Delta G = -3$ kcal mol^{-1}) for the $Ca_V1.2$ domain (Fig. 4c and Table 2). Together, these data match expectations set by the structure and underscore the importance of the N-lobe anchors to the overall affinity of Ca^{2+}/CaM for the IQ domain.

The Ca^{2+}/C-lobe binding sites for CaM and CaBP1 overlap [23] but the detailed differences in the binding modes remain unclear. To test whether the strict separation of aromatic residues into N-lobe and C-lobe anchors also held true for CaBP1, we also measured the effect that the TripleA change had on the affinities of full-length Ca^{2+}/CaBP1 and its isolated lobes. In contrast to the results with Ca^{2+}/C-lobe$_{CaM}$ (Fig. 4a), the TripleA change lowered the affinity of Ca^{2+}/C-lobe$_{CaBP1}$ for the $Ca_V1.2$ IQ domain by 1.87 kcal mol^{-1} (Fig. 4d, Table 2), suggesting that at least some of the N-lobe anchors contribute to Ca^{2+}/C-lobe$_{CaBP1}$ binding. Similarly, the TripleA change reduced the affinities of both N-lobe$_{CaBP1}$ (>5 μM, $\Delta\Delta G < -0.9$ kcal mol^{-1}) (Fig. 4e) and Ca^{2+}/CaBP1 (221 ± 14 nM, $\Delta\Delta G =$ 2.04 kcal mol^{-1}) (Fig. 4f) compared to the wild-type $Ca_V1.2$ IQ domain [23]. The impact of the TripleA change on the affinity of both Ca^{2+}/CaBP1 lobes stands in stark contrast to the results with the Ca^{2+}/CaM lobes where the affinity of Ca^{2+}/N-lobe$_{CaM}$ is reduced but that of Ca^{2+}/C-lobe$_{CaM}$ is spared (Fig. 4a). Further, the strong impact on Ca^{2+}/C-lobe$_{CaBP1}$, which has a binding site that overlaps with Ca^{2+}/C-lobe$_{CaM}$ [23], indicates that part of the Ca^{2+}/C-lobe$_{CaBP1}$ binding site includes some of the N-lobe anchors and provides evidence that the binding determinants for Ca^{2+}/CaBP1 and Ca^{2+}/CaM interactions with $Ca_V1.2$ IQ domain are not identical.

Functional competition between CaBP1 and CaM on $Ca_V1.2$

Given the biochemical evidence that CaM and CaBP1 bind to the $Ca_V1.2$ IQ domain in a mutually

exclusive way (Fig. 1e) [17,19,23], we wanted to test whether this biochemical competition could be recapitulated in a functional setting. We used two-electrode voltage clamp experiments in *Xenopus* oocytes, a system used previously to study CaBP1 function [23,47], to examine whether increasing CaM expression could overcome the functional effects of CaBP1 on $Ca_V1.2$. For these studies, we used the $Ca_V\beta_{2a}$ subunit so that there would be a negligible contribution to channel inactivation from voltage-dependent inactivation (VDI) [28]. Thus, under our experimental conditions, measurement of $Ca_V1.2$

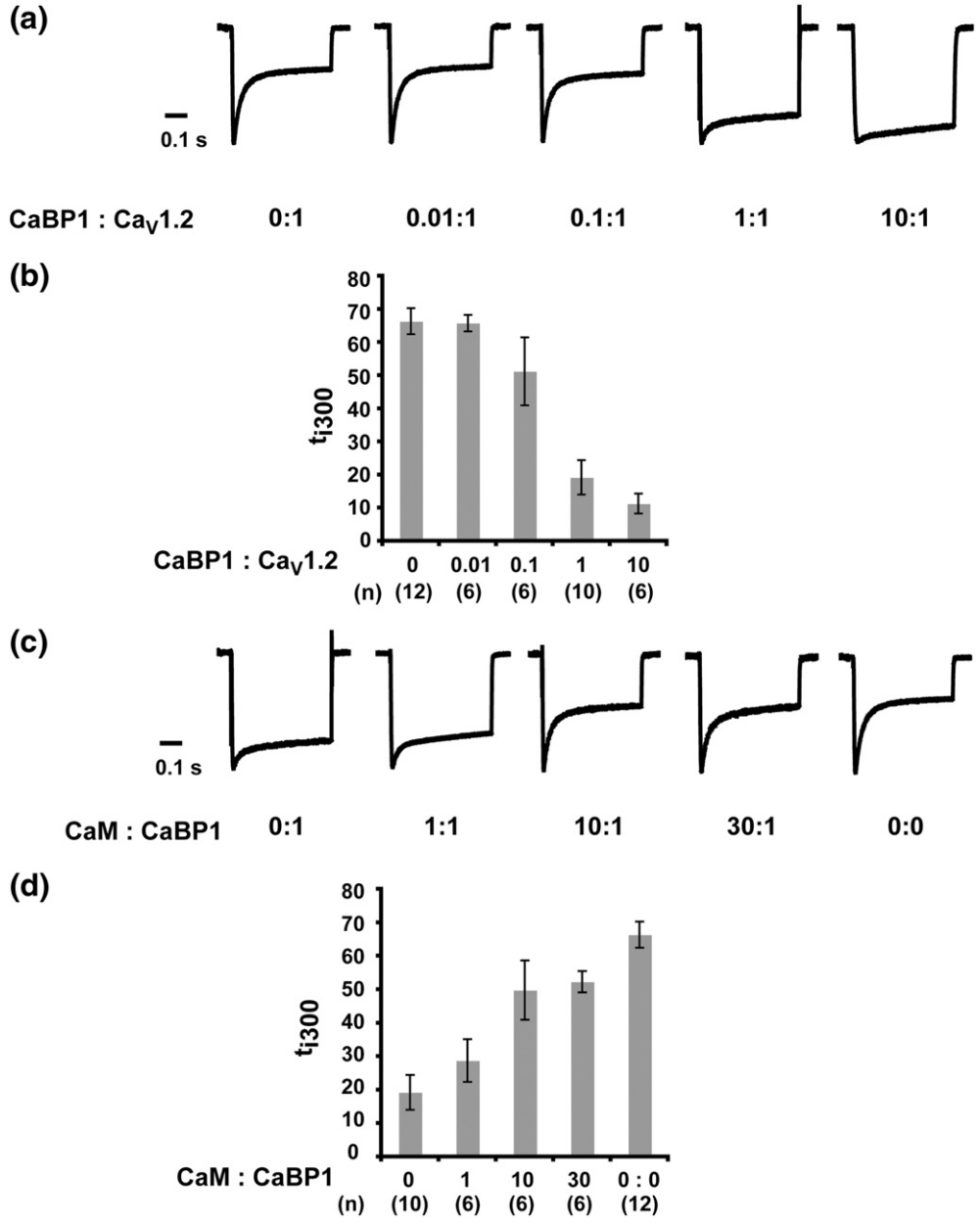

Fig. 5. CaBP1 and CaM expressed in *Xenopus* oocytes compete for control of $Ca_V1.2$ function. (a) Representative normalized I_{Ca} traces at a test potential of +20 mV for *Xenopus* oocytes co-expressing $Ca_V1.2$ and CaBP1 at the indicated ratios. (b) Averaged t_{i300} values from normalized I_{Ca} traces at a test potential of +20 mV for $Ca_V1.2$ expressed with CaBP1 at the indicated ratios. (*n*) indicates the number of experiments. (c) Representative normalized I_{Ca} traces at a test potential of +20 mV for *Xenopus* oocytes co-expressing $Ca_V1.2$ and the indicated ratios of CaBP1 and CaM. (d) Averaged t_{i300} values from normalized I_{Ca} traces at a test potential of +20 mV for $Ca_V1.2$ expressed with CaBP1 and CaM at the indicated ratio. In all experiments, RNA for $Ca_V\beta_{2a}$ and $Ca_V\alpha_2\delta$-1 was injected at concentrations equimolar to $Ca_V1.2$. (*n*) indicates the number of experiments. Trace for 1:1 CaBP1:$Ca_V1.2$ in (a) and its corresponding analysis in (b) are reproduced in (c) and (d) and labeled CaM:CaBP1 0:1.

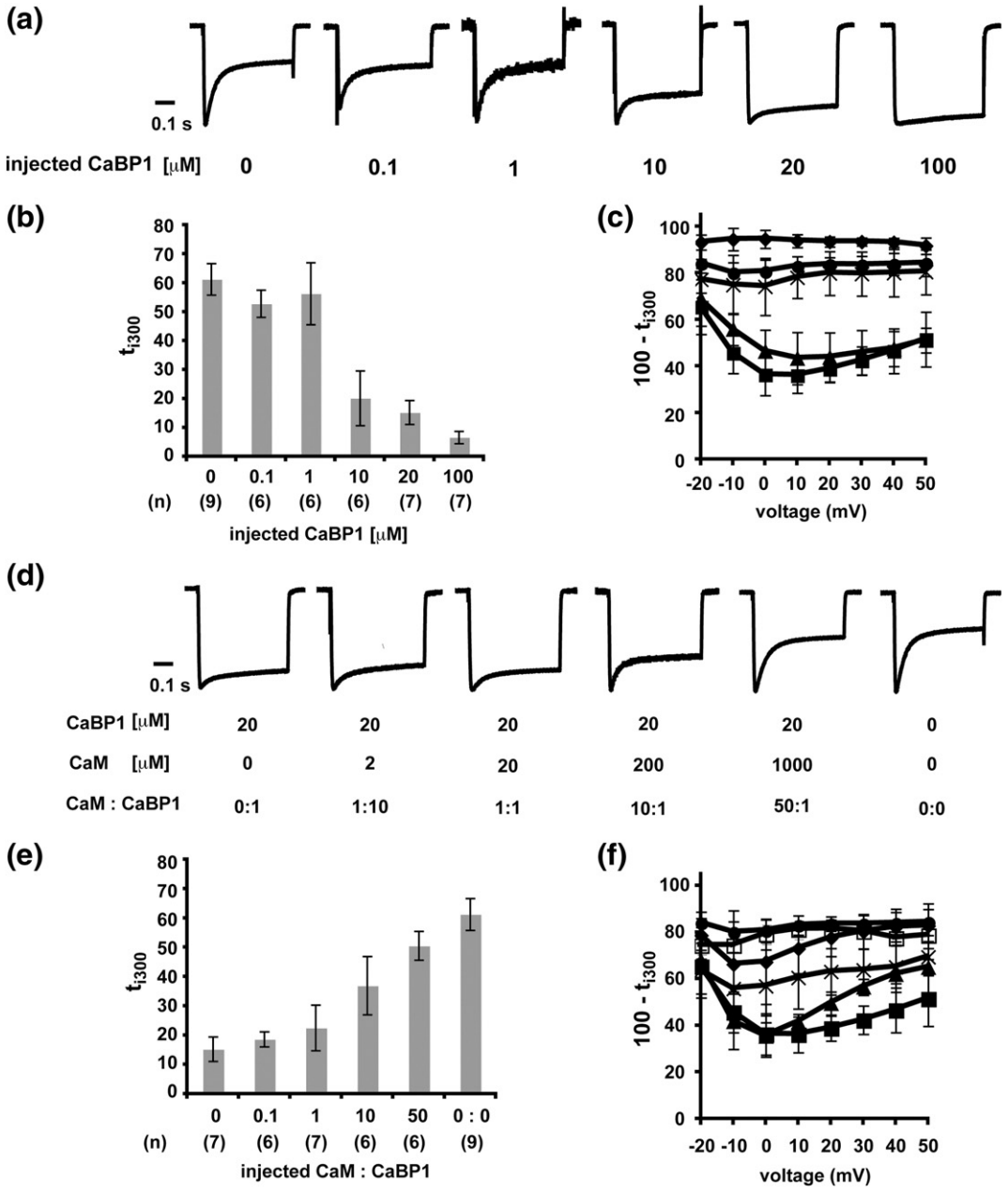

Fig. 6. Purified CaBP1 and CaM injected into cells expressing $Ca_V1.2$ compete for control of channel function. (a) Representative normalized I_{Ca} traces at a test potential of +20 mV for *Xenopus* oocytes expressing $Ca_V1.2$ and injected with 50 nl of the indicated concentrations of purified CaBP1 15 min prior to recording. (b) Averaged t_{i300} from normalized I_{Ca} traces at a test potential of +20 mV from *Xenopus* oocytes expressing $Ca_V1.2$ injected with 50 nl of CaBP1 protein at the indicated concentration 15 min prior to recording. (*n*) indicates the number of experiments. (c) Voltage dependence of the averaged normalized current 300 ms after channel activation (100 – t_{i300}) from oocytes expressing $Ca_V1.2$ and injected with purified CaBP1 at the following concentrations prior to recording: 0 μM, ■; 1 μM, ▲; 10 μM, ×; 20 μM, ●; 100 μM, ◆. (d) Representative normalized I_{Ca} traces at a test potential of +20 mV for *Xenopus* oocytes expressing $Ca_V1.2$ co-injected with the indicated concentrations of purified CaBP1 and CaM. (e) Averaged t_{i300} from normalized I_{Ca} traces at a test potential of +20 mV from oocytes expressing $Ca_V1.2$ and injected with purified CaM and CaBP1 at the indicated ratios. (*n*) indicates the number of experiments. (f) Voltage dependence of the averaged normalized current 300 ms after channel activation (100 – t_{i300}) from *Xenopus* oocytes expressing $Ca_V1.2$ and injected with purified CaM and CaBP1 1 at the following concentrations prior to recording: no CaM or CaBP1, ■; 20 μM CaBP1 only, ●; 20 μM CaBP1 and 2 μM CaM, □; 20 μM CaBP1 and 20 μM CaM, ◆; 20 μM CaBP1 and 200 μM CaM, ×; 20 μM CaBP1 and 1 mM CaM, ▲. 20 μM CaBP1 trace in (a) and its corresponding analysis in (b) and (c) are reproduced in (d), (e), and (f) and labeled as 0 μM CaM.

inactivation when calcium is the permeant ion yields a direct readout of CDI.

As a first attempt to characterize the competition between CaM and CaBP1, we pursued experiments in which CaBP1 synthesis should happen contemporaneously with that of the channel. Due to endogenous CaM, $Ca_V1.2$ CDI in oocytes is robust [6,23,30,48]. We had shown previously that even at a 60:1 excess of CaM:$Ca_V1.2$ mRNA, CaM expression did not further affect CDI as measured by the fraction of current decrease at 300 ms (t_{i300}) [49]. In contrast to these results, changes in CaBP1:$Ca_V1.2$ mRNA ratios caused clear alterations in t_{i300} and loss of CDI (Fig. 5a and b). Based on these experiments, we chose a 1:1 CaBP1:$Ca_V1.2$ mRNA ratio as the background for co-injection competition experiments with CaM mRNAs as this ratio achieved nearly full inhibition of CDI (t_{i300} = 19.3 ± 5.2%) (Fig. 5a and b). Co-injection of 1:1 CaM:CaBP1 mRNA along with the mRNAs for the other channel components resulted in recovery of a small fraction of CDI (t_{i300} = 28.8 ± 6.4%) (Fig. 5c and d). Increasing the CaM:CaBP1 ratio intensified CDI, which became nearly complete at a ratio of 30:1 CaM:CaBP1 mRNA (t_{i300} = 52.4 ± 3.2%) (Fig. 5c and d). These experiments support the idea of competitive effects between CaM and CaBP1 for control of CDI.

To test the CaM-CaBP1 competition directly and to exclude factors that might be related to differences in protein synthesis, we examined the effects on $Ca_V1.2$ CDI resulting from direct injection of purified

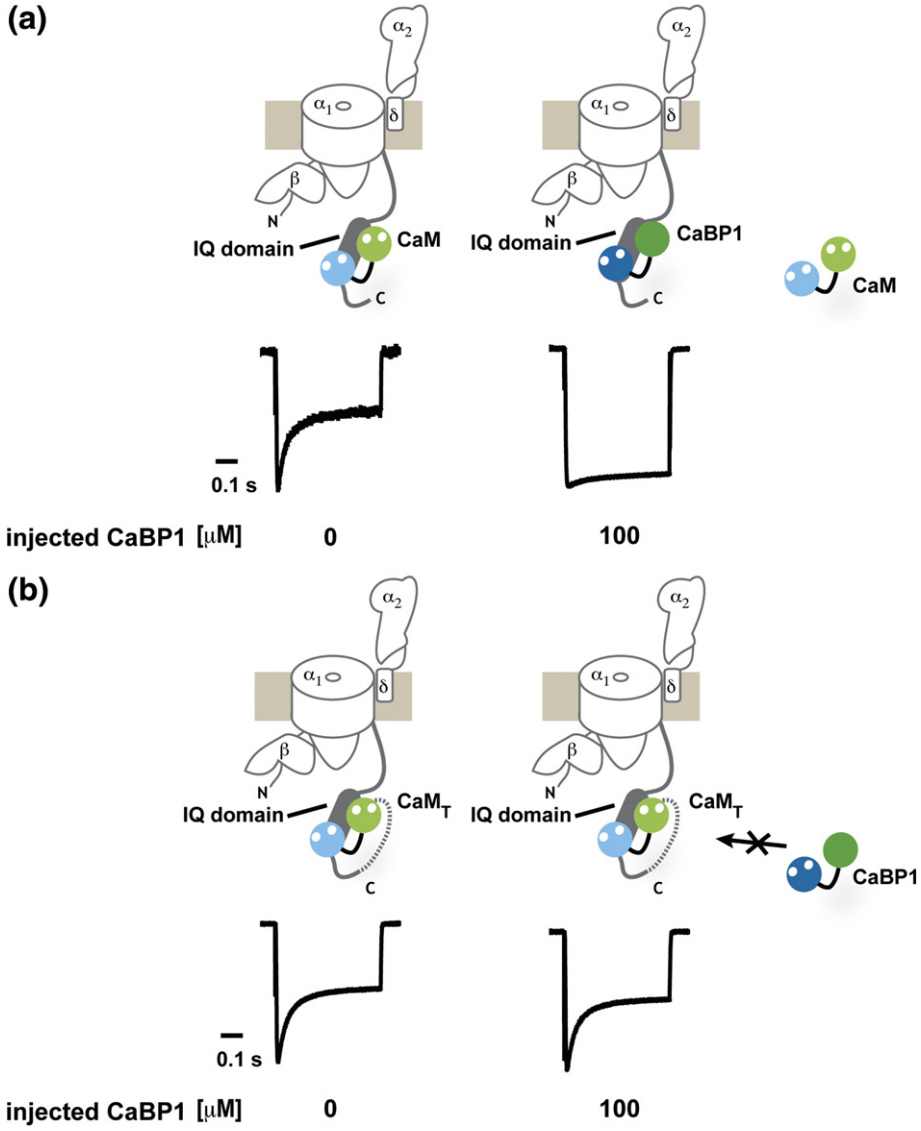

Fig. 7. $Ca_V1.2$–CaM_T channel CDI resists CaBP1 inhibition. (a) Exemplar traces of $Ca_V1.2$ with and without saturating amounts of CaBP1. The diagrams indicate Ca^{2+} channel subunits, CaM and CaBP1. (b) Exemplar traces of $Ca_V1.2$–CaM_T with the same amounts of CaBP1 as in (a).

CaBP1 and CaM protein. The proteins were injected together with 100 mM BAPTA and, thus, should be in the apo forms and remain so until the local calcium concentration is raised via voltage-dependent $Ca_V1.2$ activation. Injection of CaBP1 at concentrations of 10 μM or higher into *Xenopus* oocytes expressing $Ca_V1.2$ α_1, $Ca_V\beta_{2a}$, and $Ca_V\alpha_2\delta$-1 15 min prior to recording caused unmistakable inhibition of CDI that became nearly complete at 100 μM CaBP1 (t_{i300} = 6.6 ± 2.2%) (Fig. 6a–c). In contrast, injection of 0.1 μM or 1 μM CaBP1 or buffer alone had no effect (t_{i300} = 52.9 ± 4.7%, 56.3 ± 10.7%, and 61.2 ± 5.4%, respectively) (Fig. 6a–c). This dramatic loss of CDI indicates that the injected CaBP1 competes with endogenous CaM, which is pre-associated with the channel [38], for control of CDI.

We next asked whether co-injection of purified CaM together with CaBP1 could antagonize the CDI loss caused by CaBP1. We chose 20 μM CaBP1 as a basis level for these experiments as this concentration was the minimum required to prevent most of CDI (t_{i300} = 15.3 ± 3.2%) (Fig. 6). We found, in good agreement with the CaM and CaBP1 mRNA co-injection experiments (Fig. 5), that increasing the CaM:CaBP1 protein ratio caused a substantial recovery of CDI. This recovery became near complete when the CaM:CaBP1 ratio reached 50:1 (t_{i300} = 50.5 ± 4.9%) (Fig. 6d–f). The reciprocal effects of CaBP1 on native CaM (Fig. 6a–c) and co-injected CaM on CaBP1 (Fig. 6d–f) directly demonstrate that there is competition between CaM and CaBP1 in the context of functional Ca_V channels in a live cell membrane. Notably, this competition occurs either with the myrisotylated form of CaBP1 (Fig. 5), which causes CaBP1 to localize to membranes [50], or in the absence of this membrane anchor (Fig. 6).

Tethering CaM to $Ca_V1.2$ blocks the effects of CaBP1 on CDI

As a final test of the CaM:CaBP1 competition, we investigated the response to direct challenge by CaBP1 of a $Ca_V1.2$ construct bearing CaM that was covalently tethered to the IQ domain C-terminal end through a glycine-based linker ($Ca_V1.2$–CaM_T). This unimolecular construct is similar to one described previously [51] and should raise the CaM effective concentration to at least millimolar with respect to the IQ domain [51]. $Ca_V1.2$–CaM_T showed voltage gating and CDI and properties that were similar to wild-type untethered channels, indicating that the tethering did not greatly alter function (t_{i300} = 54.6 ± 6.2%) (Fig. 7 and Supplementary Fig. S2). However, one property was completely changed. Unlike wild-type channels for which injection of 100 μM CaBP1 prior to recording caused complete inhibition of CDI (Figs. 6a–c and 7a), CaM_T channels were totally resistant to the effects of CaBP1 injection (t_{i300} = 52.0 ± 8.2%, P = 0.56 *versus* $Ca_V1.2$–CaM_T without CaBP1 injection) (Fig. 7b). Because $Ca_V1.2$ channels bearing a tethered CaM mutant that is incapable of responding to calcium lack CDI [51], we did not pursue competition experiments of such channels with CaBP1 as there would be no functional outcome to measure. Taken together with the protein competition results (Fig. 6 and 7a), the resistance of CaM_T to the functional effects of CaBP1 provides unequivocal support for direct competition on the IQ domain between CaM and CaBP1 for control of CDI.

ITC data predict functional behavior of the apo-CaM/apo-CaBP1 competition

Although other sites have been implicated in influencing the effects of CaBP1 on channel function [25–29], our studies suggest a simple mechanism in which competition between the apo forms of CaM and CaBP1 on the Ca_V IQ domain causes channels to have or lack CDI, respectively. In order to test this conceptual model in a quantitative manner, we used the ITC-derived affinities of the apo-state and Ca^{2+}-bound forms of CaM and CaBP1 to derive the relationship between the CaM/CaBP1 ratio and the fraction of channels occupied by either the apo- or Ca^{2+}-bound forms of CaM (Appendix C) (Fig. 8). We then asked whether either curve predicts the competition measured by CDI levels from full-length functioning Ca_Vs in living cells. Strikingly, the data from the

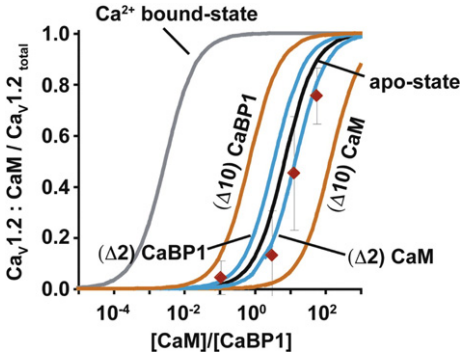

Fig. 8. Functional outcomes of CaM/CaBP1 competition for CDI match predictions based on ITC measurements. Predicted fraction of $Ca_V1.2$ channels bound to CaM as a function of [CaM]/[CaBP1] using values for the apo-state (black) and calcium-bound state (gray) IQ domain affinities measured by ITC (Table 1). Red diamonds show the fraction of CaM:$Ca_V1.2$ estimated from CDI measurements at varying ratios of injected CaM and CaBP1 protein. Teal curves show the prediction fraction of CaM-bound channels assuming that the K_d ratios of CaBP1/CaM apo states differ from the measured values by a factor of 2 in favor of CaBP, (Δ2) CaBP1, or CaM, (Δ2) CaM. Orange curves are calculated assuming that the K_d ratios of CaBP1/CaM apo states differ from the measured values by a factor of 10 in favor of CaBP, (Δ10) CaBP1, or CaM, (Δ10) CaM.

independently measured CDI values observed from our protein competition experiments (Fig. 6d and e) match exceptionally well with the curve defined by the ITC data for apo-state competition.

Even though there is a remarkably good agreement between the predicted CaM occupancy based on the *in vitro* ITC experiments and the functional competition measured on full-length channels in the membranes of living cells, other factors might affect the binding constants in the cellular setting. These might include CaM and CaBP1 binding sites located elsewhere on the channel, such as the $Ca_V1.2$ N-terminal cytoplasmic domain [22,27,47,52], or the differences in ionic composition between the *in vitro* ITC experiments and cell interior. To test the sensitivity of the mathematical model to K_d perturbations, we recalculated the relationship between the CaM/CaBP1 ratio and the fraction of channels occupied by the apo forms of CaM or CaBP1 in the case in which the K_d values differed from the measured values by a factor of 2 (Fig. 8, teal curves) (i.e., instead of $K_{d,apoCaBP1}/K_{d,apoCaM} = 7.1$, $K_{d,apoCaBP1}/K_{d,apoCaM}$ is either 3.55, a 2-fold advantage for CaBP1 relative to the measured values, or 14.2, a 2-fold advantage for CaM) or 10 (Fig. 8, orange curves) (i.e., instead of $K_{d,apoCaBP1}/K_{d,apoCaM} = 7.1$, $K_{d,apoCaBP1}/K_{d,apoCaM}$ is either 0.71, a 10-fold advantage for CaBP1, or 71, a 10-fold advantage for CaM). These comparisons clearly show that perturbations as small as 10-fold to the K_d in the setting of the cell would greatly disturb the correlation between the measured value and the predicted outcomes. These results strengthen the conclusion that the essence of the functional competition is captured by the reduced system comprising apo-CaM, apo-CaBP1, and the IQ domain and indicate that factors beyond the IQ domain have a minor role, at best, a result that agrees with the recently reported studies from Oz *et al.* [53]. Thus, a competition between the Ca^{2+}-free forms of CaM and CaBP1 occurring on a single $Ca_V1.2$ site, the IQ domain, is sufficient to explain the mechanism by which CaBP1 changes Ca_V function.

Discussion

Calcium-dependent inactivation (CDI) is a key negative feedback mechanism that determines how much calcium enters excitable cells following Ca_V voltage-dependent activation [3,4,9,54]. For $Ca_V1.2$ and $Ca_V1.3$ channels in some neurons in the brain and retina, this fundamental property can be altered dramatically by association of CaBP1 rather than CaM with the channel [16,17,19,22,55]. This change of calcium sensors has profound consequences for the frequency and duration of the Ca_V-generated intracellular calcium signals [4,5], yet the exact mechanism by which this functional alteration occurs has been unclear.

Our studies establish that there is direct competition between the apo-state forms of CaM and CaBP1 for the $Ca_V1.2$ IQ domain and that this competition controls the ability of the channel to autoregulate through CDI. This competition can be quantitatively explained based on the *in vitro*-derived ITC parameters for the interactions of the $Ca_V1.2$ IQ domain with CaM and CaBP1 (Fig. 8). The exceptionally close agreement between the *in vitro* and cell-based measurements strongly suggests that the biochemical properties of the $Ca_V1.2$ IQ domain in isolation accurately reflect the biologically relevant function of this portion of the channel. Moreover, perturbations to the K_d values as small as 10-fold eliminate this agreement between prediction and experiment. This behavioral concordance, observed in the very different contexts of an isolated biochemical system and a full-length channel complex in a living cell, is consistent with the apparent structural independence of the $Ca_V1.2$ IQ domain from other parts of the $Ca_V1.2$ C-terminal tail [26,56]. Interestingly, CaBP4, which is structurally similar to CaBP1 [23] and is able to inhibit $Ca_V1.3$ CDI [16,17], has recently been shown to compete with CaM for the $Ca_V1.4$ IQ domain and block CDI [57]. These results, together with the close conservation of Ca_V1 IQ domain sequences [8], strongly suggest that the competitive mechanism we define here is generally used by CaBP–Ca_V1 pairs.

Although apo-CaM is thought to be pre-associated with the channel complex through the IQ domain [25], the details of this interaction have remained unclear. The excellent agreement we find between the *in vitro* ITC measurements and properties of the apo-CaM:$Ca_V1.2$ IQ domain interaction measured in living cells provides strong support for the idea that CaM is associated with the IQ domain under low calcium conditions [25,32]. As the IQ domain forms a binding site having an exceptionally high affinity for Ca^{2+}/CaM, the pre-positioning of CaM on this channel element suggests that even though its conformation may change, CaM will remain tethered to the IQ domain during the entire gating cycle.

The well-documented ability of substrate interactions to change the affinity of CaM for calcium [32,40,41,43] prompted us to investigate the consequences of the sub-picomolar affinity of the Ca^{2+}/CaM:$Ca_V1.2$ IQ domain complex. Thermodynamic linkage (Fig. 3a) dictates that the very high ratio of binding constants (680,000) between Ca^{2+}/CaM and CaM for the $Ca_V1.2$ IQ domain must increase the calcium affinity of CaM in the IQ domain-bound state. Investigation of a thermodynamic model indicates that because of the high order of the reaction, the individual binding constants of each EF hand for calcium do not need to change dramatically (only ~30-fold) in order compensate for large affinity change in the complex. Hence, a large gain in the protein–protein interaction can be achieved without

a change of equivalent magnitude in calcium affinity by virtue of the multiple, coupled calcium binding sites on CaM.

The affinity of isolated CaM for calcium is in the micromolar range [42], which is outside of the response range of many Ca^{2+}/CaM-dependent protein complexes [43]. Association of CaM with the $Ca_V1.2$ IQ domain tunes the calcium response by ~30-fold into a range, 0.3–10 μM, that allows IQ domain-bound CaM to sense calcium concentrations that are much lower than expected based on free CaM and that match well with those expected for intracellular calcium changes [2,43,44]. This situation reinforces a general principle whereby CaM–substrate interactions tune the calcium-dependent response of CaM into a physiologically relevant range [41,43]. Similar analysis indicates that the reported higher intrinsic affinity of CaBP1 for Ca^{2+} relative to CaM [37] combined with the impact of association with the $Ca_V1.2$ IQ domain yields a complex that has a calcium affinity tuned near the lower limit for intracellular calcium levels [2,43,44]. This results suggests that a CaBP1:$Ca_V1.2$ IQ domain complex could be responsive to changes in Ca^{2+} levels; however, as prior studies have demonstrated that CaBP1 does not require functional EF hands to inhibit $Ca_V1.2$ CDI [23], such a response is not central to the ability of CaBP1 to block CDI.

There is a strong structural similarity between the Ca^{2+}/C-lobes of CaBP1 and CaM [23]. Although previous studies [17,19,23] suggest that the Ca^{2+}/CaBP1 and Ca^{2+}/CaM binding sites on the IQ domain overlap, the binding modes are thought to differ [23]. We show that in contrast to Ca^{2+}/CaM binding, which meets the expectations set by the structure of the Ca^{2+}/CaM:$Ca_V1.2$ IQ domain complex [30] in which Ca^{2+}/N-lobe and Ca^{2+}/C-lobe interactions are separated into two sets of aromatic anchors, some determinants of the Ca^{2+}/N-lobe$_{CaM}$ site are used by Ca^{2+}/C-lobe$_{CaBP1}$. These observations further support the notion that despite their common Ca^{2+}/C-lobe architectures [23], Ca^{2+}/CaBP1 engages the $Ca_V1.2$ IQ domain in a manner that differs from Ca^{2+}/CaM.

Our studies establish that there is direct competition between the apo-state forms of CaM and CaBP1 for the $Ca_V1.2$ IQ domain and that this simple mechanism switches the CDI properties of the channel. The demonstration that CaBP1 or CaM can be chased from channels in live cell membranes with the complementary calcium sensor (Figs. 5, 6, and 8) suggests that such competitive mechanisms may be used *in vivo* for dynamic control of Ca_V function in cells expressing CaBP1, such as hippocampal CA3 neurons [19]. In this regard, CaBP1 myristoylation, which localizes CaBP1 to membranes [50] but is not involved in CDI inhibition [23], could aid the ability of CaBP1 to compete at concentrations lower than those tested here for the non-myristoylated form (Fig. 6). Ca_V1 channels have a privileged role in excitation–transcription coupling [5,58]; hence, changes in the net calcium flux caused by substitution of CaM by CaBP1 could induce long-term effects in neuronal function. Finally, our demonstration that calcium sensors can be exchanged on pre-assembled Ca_Vs suggests that this property may enable the introduction of components bearing novel chemical reactivity to probe the conformational changes that underlie CDI.

Materials and Methods

Expression and purification

Expression and purification of CaBP1 Δ2-15 and CaM, their individual lobes, and the $Ca_V1.2$ IQ domain were as described previously [23,30]. The $Ca_V1.2$ IQ domain TripleA mutant ($Ca_V1.2$ F1618A, F1619A, Y1622A) was purified using the same procedure as for the wild-type $Ca_V1.2$ IQ domain [23,30]. CaM and CaBP1 lobes with D → A mutations at the first positions of the EF-hand consensus motif were expressed using procedures similar to those used for the wild-type counterparts [23,30]. Full-length CaM and CaBP1 with inactivated EF hands were expressed and purified similarly to the single lobes [23].

Isothermal titration calorimetry

Titrations were performed at 15 °C using a VP-ITC Microcalorimeter (MicroCal). Samples were dialyzed overnight at 4 °C (Slide-A-Lyzer, 2 kDa molecular mass cutoff, Thermo Scientific) against appropriate buffers. Titrations were conducted in 5 mM KCl, 1 mM $CaCl_2$, and 10 mM Hepes, pH 7.4. After centrifugation at 40,000 rpm for 30 min at 4 °C, protein concentration was determined by absorbance at 280 nm [59]. In cases where precipitation at high concentrations of the syringe component precluded direct titration experiments, such as the EF hand mutants, we used a displacement ITC strategy [23,31]. All samples were degassed for 5 min prior to loading into the calorimeter. Each ITC experiment consisted of one 4-μl injection followed by 29 injections of 10 μl of titrant. Either heat of dilution from titrations of injectant into buffer was subtracted or the final titration points were used to estimate/correct the baseline. Data were processed with MicroCal Origin 7.0 using the binding models indicated in the main text.

Electrophysiology

Human $Ca_V1.2$ (α_1C77, GenBank CAA84346), rat $Ca_V\beta_{2a}$ (GenBank NP 446303), and $Ca_V\alpha_2\delta$-1(GenBank NM_00182276), co-expressed with either *Homo sapiens* CaM (GenBank NM_006888) or the short isoform of *H. sapiens* CaBP1 (GenBank AF169148), which bears a myristoylation site, were used for two-electrode voltage clamp experiments in *Xenopus* oocytes. Details of constructs and two-electrode voltage clamp have been described previously [23]. In short, linearized cDNA was

translated into capped mRNA using the T7 mMessenger kit (Ambion). Fifty nanoliters of $Ca_V\alpha_1$, $Ca_V\beta$, $Ca_V\alpha_2\delta$-1, and CaBP1 or CaM mRNA at the molar ratio indicated were injected into stage VI *Xenopus* oocytes. For experiments that involved protein injections into oocytes, equimolar mRNA of $Ca_V\alpha_1$, $Ca_V\beta$, and $Ca_V\alpha_2\delta$-1 were injected 48 h prior to recording. Fifteen minutes before recording, 50 nl of a mixture of 0.1 M BAPTA and the test proteins at the indicated concentrations were injected. The $Ca_V1.2$ tethered CaM construct ($Ca_V1.2$–CaM_T) consists of residues 1–1644 of human $Ca_V1.2$, followed by a six-residue linker (TGGGGG) and residues 1–147 of human CaM. This linker, together with the six disordered residues from the $Ca^{2+}{}_4$:CaM N-terminus and $Ca_V1.2$ IQ C-terminus [30], provides sufficient length to span the required distance in a manner compatible with the structure in PDB:2BE6.

Two-electrode voltage-clamp experiments were performed 2 to 3 days post-injection. Oocytes were injected with 50 nl of 100 mM BAPTA 4 min before recording unless stated otherwise to minimize calcium-activated chloride currents. Recording solutions contained 40 mM $Ca(NO_3)_2$, 50 mM NaOH, 1 mM KOH, and 10 mM Hepes, adjusted to pH 7.4 using HNO_3. Electrodes were filled with 3 M KCl and had resistances of 0.3–2.0 MΩ. CDI was measured using 450-ms depolarizations from a −90 mV holding potential to test potentials of −50 to +50 mV in 10-mV steps. Consecutive pulses were separated by 15 s. Leak currents were subtracted using a P/4 protocol. Currents were analyzed with Clampfit 8.2 (Axon Instruments). All results are from at least two independent oocyte batches. The t_{i300} values were calculated from normalized currents at +20 mV and represent the percentage inactivation after 300 ms.

Acknowledgements

This work was supported by grants from the National Institutes of Health (R01 HL080050) and the American Heart Association (0740019N) to D.L.M. We thank R. Aldrich and M. Grabe for critical comments on the manuscript, and members of the Minor laboratory for support throughout these studies. D.L.M. is an American Heart Association Established Investigator.

Supplementary Data

Supplementary data to this article can be found online at http://dx.doi.org/10.1016/j.jmb.2013.06.024

Appendix A

We modeled the system of CaM, calcium, and the IQ domain using a thermodynamic cycle (Fig. 3a) governed by the following equations:

$$K_1 = \left(\left[Ca^{2+}\right]^4[CaM]\right)/\left[Ca^{2+}{}_4 : CaM\right] \quad (A1)$$

$$K_2 = ([IQ][CaM])/[CaM : IQ] \quad (A2)$$

$$K_3 = \left([IQ]\left[Ca^{2+}{}_4 : CaM\right]\right)/\left[Ca^{2+}{}_4 : CaM : IQ\right] \quad (A3)$$

$$K_4 = \left(\left[Ca^{2+}\right]^4[CaM : IQ]\right)/\left[Ca^{2+}{}_4 : CaM : IQ\right] \quad (A4)$$

Conservation of free energy dictates that the free-energy difference of Ca^{2+} binding is as follows:

$$\Delta\Delta G = \Delta G_2 - \Delta G_3 = \Delta G_1 - \Delta G_4. \quad (A5)$$

Consequently, knowing the free-energy values of the individual binding reactions for the calcium-bound and calcium-free forms of CaM with the IQ domain, ΔG_2 and ΔG_3, dictates the difference in calcium affinity ($\Delta\Delta G_{CaM}$) for reactions ΔG_1 and ΔG_4.

The values of ΔG_2 and ΔG_3 are as follows:

$$\Delta G_2 = -8.10 \text{ kcal mol}^{-1} \quad (A6)$$

(Fig. 2c and Table 1)

$$\Delta G_3 = -15.68 \text{ kcal mol}^{-1} \quad (A7)$$

(Fig. 1b and Table 1). Thus, combining Eq. (A5) with Eqs. (A6) and (A7) yields the free-energy difference corresponding to:

$$\Delta\Delta G_{CaM} = \Delta G_1 - \Delta G_4 = 7.58 \text{ kcal mol}^{-1}. \quad (A8)$$

$\Delta\Delta G$ comprises the individual Ca^{2+} affinities of the four EF hands rather than a single binding reaction. Making the simplifying assumption that all CaM EF hands are affected equally by binding of the IQ domain results in each EF-hand free-energy difference altered by 1.90 kcal mol^{-1}, one-fourth of the total free energy difference of 7.58 kcal mol^{-1}, at 288 K, an increase of 28.8-fold in the calcium affinity of each individual EF hand. Although the CaM EF hands may not be affected equally, in the context of the limits set by the thermodynamic cycle (Fig. 3a), any unequal changes in EF-hand affinity would result in only modest changes in the relation shown in Fig. 3b.

Appendix B

We modeled the system of CaBP1, calcium, and the IQ domain using a thermodynamic cycle (Supplementary Fig. S1), using an equivalent analysis to that presented in Appendix A for CaM as follows:

$$K_1 = \left(\left[Ca^{2+}\right]^2[CaBP1]\right)/\left[Ca^{2+}{}_2 : CaBP1\right] \quad (B1)$$

$$K_2 = ([IQ][CaBP1])/[CaBP1 : IQ] \quad (B2)$$

$$K_3 = \left([IQ]\left[Ca^{2+}{}_2 : CaBP1\right]\right)/\left[Ca^{2+}{}_2 : CaBP1 : IQ\right] \quad (B3)$$

$$K_4 = \left(\left[Ca^{2+}\right]^2[CaBP1 : IQ]\right)/\left[Ca^{2+}{}_2 : CaBP1 : IQ\right] \quad (B4)$$

For CaBP1, the values of ΔG_2 and ΔG_3 are as follows:

$$\Delta G_2 = -9.15 \text{ kcal mol}^{-1} \quad (B5)$$

(Table 1 and Fig. 2e)

$$\Delta G_3 = -12.38 \text{ kcal mol}^{-1} \quad (B6)$$

(Table 1 and Ref. [23]). Thus, combining Eq. (A5) with Eqs. (B5) and (B6) yields a difference of free-energy corresponding to:

$$\Delta\Delta G_{CaBP}1 = \Delta G_1 - \Delta G_4 = 3.23 \text{ kcal mol}^{-1} \quad (B7)$$

Making the simplifying assumption that both functional CaBP1 EF hands are affected equally by binding of the IQ domain specifies that each EF-hand free-energy difference is altered by 1.62 kcal mol^{-1}, half of 3.23 kcal mol^{-1}, equivalent to an increase of 17.5-fold in the calcium affinity of each individual EF hand.

Appendix C

The ITC data (Fig. 1 and Table 1) dictate the following relationships for the calcium-bound forms of CaM and CaBP1:

$$K_{d,CaM} = [IQ][CaM]/[CaM : IQ] = 850 \text{ fM} \quad (C1)$$

and

$$K_{d,CaBP1} = [IQ][CaBP1]/[CaBP1 : IQ] = 290 \text{ pM} \quad (C2)$$

Dividing Eq. (C1) by Eq. (C2) gives:

$$K_{d,CaM}/K_{d,CaBP1} = [CaM][CaBP1 : IQ]/[CaM : IQ][CaBP1] = 0.0029 \quad (C3)$$

Rearranging this equation to yield the ratio between the IQ domains occupied by the two Ca^{2+} sensors yields:

$$[CaM]/[CaBP1] = 0.0029\,[CaM : IQ]/[CaBP1 : IQ] \quad (C4)$$

which can be solved for any given ratio of CaM and CaBP1.

We assume that competition between CaBP1 and CaM occurs exclusively on the $Ca_V1.2$ IQ domain, allowing us to substitute the full-length channel for the IQ domain.

$$[CaM : Ca_V1.2]/[CaBP1 : Ca_V1.2] = 0.0029\,[CaM]/[CaBP1] \quad (C5)$$

This assumption ignores the possible influence of other sites on $Ca_V1.2$ that have been shown to have affinity for both CaM [25,27] and CaBP1 [19,22]. Notably, such sites have a >5-fold weaker affinity than the $Ca_V1.2$ IQ domain for CaM [32,52].

We furthermore assume that there is always one calcium sensor bound to the $Ca_V1.2$ IQ domain; that is,

$$[Ca_V1.2]_{total} = [CaBP1{:}Ca_V1.2] + [CaM{:}Ca_V1.2] \quad (C6)$$

For Eq. (C6), given that without CaM, $Ca_V1.2$ trafficking to the plasma membrane is heavily compromised [60], we assume that the amount of $Ca_V1.2$ in the plasma membrane of the test *Xenopus* oocyte lacking either calcium sensor is negligible.

Similar analysis for the apo-state values (Fig. 2 and Table 1) yields the following equations:

$$[CaMEF1234]/[CaBP1EF34] = 7.1\,[CaBP1EF34/IQ]/[CaMEF1234/IQ] \quad (C7)$$

and

$$[CaMEF1234]/[CaBP1EF34] = 7.1\,[CaBP1EF34{:}Ca_V1.2]/[CaMEF1234{:}Ca_V1.2] \quad (C8)$$

Equations (C5) and (C8) can be used to derive the relationship between the CaM/CaBP1 ratio and the fraction of the channel occupied by CaM in high (Fig. 8, gray curve) and low Ca^{2+} (Fig. 8, black curve).

Received 21 April 2013;
Received in revised form 12 June 2013;
Accepted 18 June 2013
Available online 25 June 2013

Keywords:
voltage-gated calcium channel;
isothermal titration calorimetry;
electrophysiology;
calcium sensor proteins;
mathematical models

Abbreviations used:
CaM, calmodulin; CaBP1, calcium-binding protein 1; CDI, calcium-dependent inactivation; ITC, isothermal titration calorimetry; C-lobe, C-terminal lobe; N-lobe, N-terminal lobe.

References

[1] Catterall WA. Structure and regulation of voltage-gated Ca^{2+} channels. Annu Rev Cell Dev Biol 2000;16:521–55.
[2] Clapham DE. Calcium signaling. Cell 2007;131:1047–58.
[3] Dunlap K. Calcium channels are models of self-control. J Gen Physiol 2007;129:379–83.
[4] Christel C, Lee A. Ca(2+)-dependent modulation of voltage-gated Ca(2+) channels. Biochim Biophys Acta 2011;1820:1243–52.
[5] Wheeler DG, Groth RD, Ma H, Barrett CF, Owen SF, Safa P, et al. Ca(V)1 and Ca(V)2 channels engage distinct modes of Ca(2+) signaling to control CREB-dependent gene expression. Cell 2012;149:1112–24.
[6] Zühlke RD, Pitt GS, Deisseroth K, Tsien RW, Reuter H. Calmodulin supports both inactivation and facilitation of L-type calcium channels. Nature 1999;399:159–62.
[7] Peterson BZ, DeMaria CD, Adelman JP, Yue DT. Calmodulin is the Ca^{2+} sensor for Ca^{2+}-dependent inactivation of L-type calcium channels. Neuron 1999;22:549–58.
[8] Van Petegem F, Minor DL. The structural biology of voltage-gated calcium channel function and regulation. Biochem Soc Trans 2006;34:887–93.
[9] Findeisen F, Minor Jr DL. Progress in the structural understanding of voltage-gated calcium channel (CaV) function and modulation. Channels (Austin) 2010;4:459–74.
[10] Dolphin AC. beta subunits of voltage-gated calcium channels. J Bioenerg Biomembr 2003;35:599–620.
[11] Buraei Z, Yang J. The beta subunit of voltage-gated Ca^{2+} channels. Physiol Rev 2010;90:1461–506.
[12] Davies A, Hendrich J, Van Minh AT, Wratten J, Douglas L, Dolphin AC. Functional biology of the alpha(2)delta subunits of voltage-gated calcium channels. Trends Pharmacol Sci 2007;28:220–8.
[13] Pitt GS. Calmodulin and CaMKII as molecular switches for cardiac ion channels. Cardiovasc Res 2007;73:641–7.
[14] McCue HV, Haynes LP, Burgoyne RD. The diversity of calcium sensor proteins in the regulation of neuronal function. Cold Spring Harbor Perspect Biol 2010;2:a004085.
[15] Haeseleer F, Sokal I, Verlinde CL, Erdjument-Bromage H, Tempst P, Pronin AN, et al. Five members of a novel Ca(2+)-binding protein (CABP) subfamily with similarity to calmodulin. J Biol Chem 2000;275:1247–60.
[16] Cui G, Meyer AC, Calin-Jageman I, Neef J, Haeseleer F, Moser T, et al. Ca^{2+}-binding proteins tune Ca^{2+}-feedback to Cav1.3 channels in mouse auditory hair cells. J Physiol 2007;585:791–803.
[17] Yang PS, Alseikhan BA, Hiel H, Grant L, Mori MX, Yang W, et al. Switching of Ca^{2+}-dependent inactivation of Ca(v)1.3 channels by calcium binding proteins of auditory hair cells. J Neurosci 2006;26:10677–89.
[18] Lee A, Westenbroek RE, Haeseleer F, Palczewski K, Scheuer T, Catterall WA. Differential modulation of Ca(v)2.1 channels by calmodulin and Ca^{2+}-binding protein 1. Nat Neurosci 2002;5:210–7.
[19] Zhou H, Kim SA, Kirk EA, Tippens AL, Sun H, Haeseleer F, et al. Ca^{2+}-binding protein-1 facilitates and forms a postsynaptic complex with Cav1.2 (L-type) Ca^{2+} channels. J Neurosci 2004;24:4698–708.
[20] Few AP, Lautermilch NJ, Westenbroek RE, Scheuer T, Catterall WA. Differential regulation of CaV2.1 channels by calcium-binding protein 1 and visinin-like protein-2 requires N-terminal myristoylation. J Neurosci 2005;25:7071–80.
[21] Lautermilch NJ, Few AP, Scheuer T, Catterall WA. Modulation of CaV2.1 channels by the neuronal calcium-binding protein visinin-like protein-2. J Neurosci 2005;25:7062–70.
[22] Zhou H, Yu K, McCoy KL, Lee A. Molecular mechanism for divergent regulation of Cav1.2 Ca^{2+} channels by calmodulin and Ca^{2+}-binding protein-1. J Biol Chem 2005;280:29612–9.
[23] Findeisen F, Minor Jr DL. Structural basis for the differential effects of CaBP1 and calmodulin on Ca(V)1.2 calcium-dependent inactivation. Structure 2010;18:1617–31.
[24] Li C, Chan J, Haeseleer F, Mikoshiba K, Palczewski K, Ikura M, et al. Structural insights into Ca^{2+}-dependent regulation of inositol 1,4,5-trisphosphate receptors by CaBP1. J Biol Chem 2009;284:2472–81.
[25] Erickson MG, Liang H, Mori MX, Yue DT. FRET two-hybrid mapping reveals function and location of L-type Ca^{2+} channel CaM preassociation. Neuron 2003;39:97–107.
[26] Kim EY, Rumpf CH, Van Petegem F, Arant RJ, Findeisen F, Cooley ES, et al. Multiple C-terminal tail Ca(2+)/CaMs regulate Ca(V)1.2 function but do not mediate channel dimerization. EMBO J 2010;29:3924–38.
[27] Dick IE, Tadross MR, Liang H, Tay LH, Yang W, Yue DT. A modular switch for spatial Ca^{2+} selectivity in the calmodulin regulation of CaV channels. Nature 2008;451:830–4.
[28] Findeisen F, Minor Jr DL. Disruption of the IS6-AID linker affects voltage-gated calcium channel inactivation and facilitation. J Gen Physiol 2009;133:327–43.
[29] Ravindran A, Lao QZ, Harry JB, Abrahimi P, Kobrinsky E, Soldatov NM. Calmodulin-dependent gating of Ca(v)1.2 calcium channels in the absence of Ca(v)beta subunits. Proc Natl Acad Sci USA 2008;105:8154–9.
[30] Van Petegem F, Chatelain FC, Minor Jr DL. Insights into voltage-gated calcium channel regulation from the structure of the CaV1.2 IQ domain-Ca^{2+}/calmodulin complex. Nat Struct Mol Biol 2005;12:1108–15.
[31] Sigurskjold BW. Exact analysis of competition ligand binding by displacement isothermal titration calorimetry. Anal Biochem 2000;277:260–6.
[32] Evans TI, Hell JW, Shea MA. Thermodynamic linkage between calmodulin domains binding calcium and contiguous sites in the C-terminal tail of Ca(V)1.2. Biophys Chem 2011;159:172–87.
[33] Fallon JL, Halling DB, Hamilton SL, Quiocho FA. Structure of calmodulin bound to the hydrophobic IQ domain of the cardiac Ca(v)1.2 calcium channel. Structure 2005;13:1881–6.
[34] Tse JK, Giannetti AM, Bradshaw JM. Thermodynamics of calmodulin trapping by Ca^{2+}/calmodulin-dependent protein kinase II: subpicomolar Kd determined using competition titration calorimetry. Biochemistry 2007;46:4017–27.
[35] Sarhan MF, Tung CC, Van Petegem F, Ahern CA. Crystallographic basis for calcium regulation of sodium channels. Proc Natl Acad Sci USA 2012;109:3558–63.
[36] Sarhan MF, Van Petegem F, Ahern CA. A double tyrosine motif in the cardiac sodium channel domain III–IV linker couples calcium-dependent calmodulin binding to inactivation gating. J Biol Chem 2009;284:33265–74.
[37] Wingard JN, Chan J, Bosanac I, Haeseleer F, Palczewski K, Ikura M, et al. Structural analysis of Mg^{2+} and Ca^{2+} binding to

CaBP1, a neuron-specific regulator of calcium channels. J Biol Chem 2005;280:37461–70.
[38] Erickson MG, Alseikhan BA, Peterson BZ, Yue DT. Preassociation of calmodulin with voltage-gated Ca(2+) channels revealed by FRET in single living cells. Neuron 2001;31:973–85.
[39] Tang W, Halling DB, Black DJ, Pate P, Zhang JZ, Pedersen S, et al. Apocalmodulin and Ca^{2+} calmodulin-binding sites on the CaV1.2 channel. Biophys J 2003;85:1538–47.
[40] Milos M, Schaer JJ, Comte M, Cox JA. Microcalorimetric investigation of the interactions in the ternary complex calmodulin–calcium–melittin. J Biol Chem 1987;262:2746–9.
[41] Zhang M, Abrams C, Wang LP, Gizzi A, He LP, Lin RH, et al. Structural basis for calmodulin as a dynamic calcium sensor. Structure 2012;20:911–23.
[42] Linse S, Helmersson A, Forsen S. Calcium binding to calmodulin and its globular domains. J Biol Chem 1991;266:8050–4.
[43] Xia Z, Storm DR. The role of calmodulin as a signal integrator for synaptic plasticity. Nat Rev Neurosci 2005;6:267–76.
[44] Hille B. Ion Channels of Excitable Membranes. 3rd edit. Sunderland, MA: Sinauer Associates, Inc; 2001 .
[45] Chao LH, Stratton MM, Lee IH, Rosenberg OS, Levitz J, Mandell DJ, et al. A mechanism for tunable autoinhibition in the structure of a human Ca^{2+}/calmodulin-dependent kinase II holoenzyme. Cell 2011;146:732–45.
[46] Chiba H, Schneider NS, Matsuoka S, Noma A. A simulation study on the activation of cardiac CaMKII delta-isoform and its regulation by phosphatases. Biophys J 2008;95:2139–49.
[47] Oz S, Tsemakhovich V, Christel CJ, Lee A, Dascal N. CaBP1 regulates voltage-dependent inactivation and activation of Ca(V)1.2 (L-type) calcium channels. J Biol Chem 2011;286:13945–53.
[48] Ivanina T, Blumenstein Y, Shistik E, Barzilai R, Dascal N. Modulation of L-type Ca^{2+} channels by gbeta gamma and calmodulin via interactions with N and C termini of alpha 1C. J Biol Chem 2000;275:39846–54.
[49] Findeisen F, Tolia A, Arant R, Kim EY, Isacoff E, Minor Jr DL. Calmodulin overexpression does not alter Cav1.2 function or oligomerization state. Channels (Austin) 2011;5:320–4.
[50] Haynes LP, Tepikin AV, Burgoyne RD. Calcium-binding protein 1 is an inhibitor of agonist-evoked, inositol 1,4,5-trisphosphate-mediated calcium signaling. J Biol Chem 2004;279:547–55.
[51] Mori MX, Erickson MG, Yue DT. Functional stoichiometry and local enrichment of calmodulin interacting with Ca^{2+} channels. Science 2004;304:432–5.
[52] Benmocha A, Almagor L, Oz S, Hirsch JA, Dascal N. Characterization of the calmodulin-binding site in the N terminus of CaV1.2. Channels (Austin) 2009;3:337–42.
[53] Oz S, Benmocha A, Sasson Y, Sachyani D, Almagor L, Lee A, et al. Competitive and non-competitive regulation of calcium-dependent inactivation in CaV1.2L-type Ca^{2+} channels by calmodulin and Ca^{2+}-binding protein 1. J Biol Chem 2013;288:12680–91.
[54] Halling DB, Aracena-Parks P, Hamilton SL. Regulation of voltage-gated Ca^{2+} channels by calmodulin. Sci STKE 2006;2006:er1.
[55] Haeseleer F, Imanishi Y, Maeda T, Possin DE, Maeda A, Lee A, et al. Essential role of Ca^{2+}-binding protein 4, a Cav1.4 channel regulator, in photoreceptor synaptic function. Nat Neurosci 2004;7:1079–87.
[56] Fallon JL, Baker MR, Xiong L, Loy RE, Yang G, Dirksen RT, et al. Crystal structure of dimeric cardiac L-type calcium channel regulatory domains bridged by Ca^{2+*} calmodulins. Proc Natl Acad Sci USA 2009;106:5135–40.
[57] Shaltiel L, Paparizos C, Fenske S, Hassan S, Gruner C, Rotzer K, et al. Complex regulation of voltage-dependent activation and inactivation properties of retinal voltage-gated Cav1.4L-type Ca^{2+} channels by Ca^{2+}-binding protein 4 (CaBP4). J Biol Chem 2012;287:36312–21.
[58] Murphy TH, Worley PF, Baraban JM. L-type voltage-sensitive calcium channels mediate synaptic activation of immediate early genes. Neuron 1991;7:625–35.
[59] Edelhoch H. Spectroscopic determination of tryptophan and tyrosine in proteins. Biochemistry 1967;6:1948–54.
[60] Wang HG, George MS, Kim J, Wang C, Pitt GS. Ca^{2+}/-calmodulin regulates trafficking of Ca(V)1.2 Ca^{2+} channels in cultured hippocampal neurons. J Neurosci 2007;27:9086–93.